MASTER OF SCIENCE

DRG2 depletion promotes endothelial cell senescence and vascular endothelial dysfunction

The Graduate School of the University of Ulsan

Department of Biological Science

Le Anh Nhung

DRG2 depletion promotes endothelial cell senescence and vascular endothelial dysfunction

Supervisor: Professor Jeong Woo Park, Ph.D.

A Dissertation

Submitted to
the Graduate School of the University of Ulsan
In partial Fulfillment of the Requirements
for the Degree of

Master of Science

by

Le Anh Nhung

Department of Biological Science
University of Ulsan, Korea
May 2022

DRG2 depletion promotes endothelial cell senescence and vascular endothelial dysfunction

This certifies that the master thesis of Le Anh Nhung is approved by

Committee Chair Professor. 이병주

Committee Member Professor. 백승훈

Committee Member Professor. 박정우

Department of Biological Science
University of Ulsan, Korea
May 2022

Abstract

Endothelial cell senescence is involved in the endothelial dysfunction and vascular diseases. However, detailed mechanisms involved in endothelial senescence are not fully understood. Here, we demonstrated that deficiency of developmentally regulated GTP-binding protein 2 (DRG2) induces senescence and dysfunction of endothelial cells. DRG2 knockout (KO) mice displayed reduced blood flow in cerebral brain and reduced lung blood vessel density. We also found that DRG2 deficiency reduced angiogenic capability of endothelial cells determined by matrigel plug assay, aorta ring assay, and in vitro tubule formation of primary lung endothelial cells. Endothelial cells from DRG2 KO mice showed a senescence phenotype, including decreased cell growth, and enhanced level of p21 and phosphorylated p53, γH2AX, senescence-associated β-galactosidase (SA-β-gal) activity, and SASP cytokines. DRG2 deficiency in endothelial cells upregulated arginase 2 (Arg2) and reactive oxygen species (ROS) production. Induction of SA-β-gal activity was prevented by the anti-oxidant N-acetyl cysteine (NAC) in endothelial cells from DRG2 KO mice. In conclusion, our results suggest that DRG2 is a key regulator of endothelial senescence and downregulation of DRG2 is likely involved in vascular dysfunction and vascular diseases.

Key words: DRG2, endothelial cells, senescence, angiogenesis, vascular dysfunction

Contents

List of Figures

I. INTRODUCTION

Endothelial cells form the inner lining of the vasculature and regulate blood flow in vascular circulation [1], thus playing a pivotal role in vascular function [2]. Angiogenesis, the formation of new capillaries from pre-existing blood, is primarily carried out by endothelial cells, the innermost layer of blood vessels [3]. Endothelial dysfunction impairs angiogenesis and contributes to the increased prevalence of cardiovascular diseases [4]. Thus, understanding the basis of impaired angiogenesis and endothelial dysfunction has important implications for understanding and managing cardiovascular disease.

Cellular senescence is characterized by a cell-cycle arrest and pro-inflammatory changes in gene expression [5]. Senescence of endothelial cells leads to endothelial dysfunction and impaired angiogenesis [6]. Senescence can be induced by various kinds of stimuli, including ionizing radiation [7], telomere dysfunction [8] or reactive oxygen species (ROS) [9]. Among them, oxidative stress plays a central role in the development of cellular senescence [10]. Oxidative stress occurs when the production of reactive oxygen species (ROS) overwhelms endogenous antioxidant systems and/or when the endogenous antioxidant systems are impaired. ROS are a group of oxygen-based molecules characterized by their high chemical reactivity [11], [12]. Although oxidative stress is one of the major factors causing the onset of senescence [13], the specific mechanisms underlying ROS-induced endothelial senescence are not completely clear.

In the endothelium, endothelial nitric oxide synthase (eNOS) uses L-arginine as a substrate to produce NO which plays a protective physiological role in the vasculature [14]. Arginase 2 (Arg2), a predominant isoform of arginase in endothelial cells [15], also utilizes L-arginine and, thereby, directly competes with eNOS for L-arginine and inhibits NO synthesis

by competing with eNOS for L-arginine [16]. Upregulation of Arg2 decreases intracellular L-arginine content and reduces NO production and increases the production of ROS by eNOS uncoupling [17], [18]. Thus, Arg2 plays an important role in endothelial dysfunction with implications in vascular disease [19].

Developmentally regulated GTP-binding proteins (DRGs) constitute a subfamily of the GTPase superfamily [20]. The DRG subfamily consists of two closely related proteins, DRG1 and DRG2 [21]. DRG1 and DRG2 interacts with different molecules, DFRP1 and DFRP2, respectively [22, p. 2], suggesting that they have distinct functions. Previously, we found that overexpression of DRG2 affects cell proliferation and apoptosis in Jurkat human T cells [23], [24], inhibits T_H17 differentiation, and ameliorates experimental autoimmune encephalomyelitis in mice [25]. We also learned that DRG2 interacts with Rab5 on endosomes and is required for Rab5 inactivation on endosomes and for recycling of transferrin (Tfn) to the plasma membrane [26]. Recently, it has been shown that DRG2 knockdown induces golgi fragmentation [27] and mitochondrial dysfunction [28, p. 1], decreases the stability of Rac1-positive membrane tubules in cancer cells [29], and suppresses VEGF-A production from melanoma cells, leading to inhibition of tumor angiogenesis [30]. Knocking out of DRG2 impairs dopamine release from dopamine neuron in mouse brain [31]. Together, these data demonstrate that DRG2 is an important regulator of signal pathways for cell growth, differentiation, and/or vesicle trafficking. However, little is known about the functional role of DRGs in endothelial cells.

In this study, we examined the role of DRG2 in the regulation of endothelial generation of ROS and endothelial senescence. We demonstrated that DRG2 depletion increases NOX2 expression, ROS generation, and senescence in endothelial cells. In addition, we found that DRG2 deficiency reduces angiogenic activity of endothelial cells, lung blood vessel density,

and blood flow in cerebral brain. Together, these results suggest that DRG2 deficiency leads to endothelial dysfunction and impaired angiogenesis through upregulation of ROS and senescence in endothelial cells.

II. MATERIALS AND METHODS

2.1 Cell culture

Mouse lung endothelial cells (mLECs) were isolated by methods as previously described [30]. Briefly, cell suspensions were prepared by digesting mouse lungs in collagenase and incubated with anti-CD31 monoclonal antibody for 30 min at 4ºC. Cells were pulled down using magnetic beads coated with sheep anti-IgG. After washing four times, cells were digested with trypsin-EDTA to detach the beads. Cells were cultured in Dulbecco's Modified Eagle (DMEM) (Life Technologies) supplemented with 15% fetal bovine serum (FBS; Thermo Scientific), heparin (100 μg/ml) (Sigma), 100 U/ml penicillin, and 100 μg/ml streptomycin (Gibco) and cultured in 2% gelatin (Sigma)-coated plate at 37°C and 5% CO_2.

2.2 Mice and animal research ethics

DRG2$^{-/-}$ mice were described previously [26]. Mice were bred in the animal facility at the University of Ulsan, and offspring were born and housed in the same room under specific pathogen-free conditions. All mice were handled in accordance with the Guide for the Care and Use of Laboratory Animals from the National Research Council. All animal procedures were approved by the Institutional Animal Care and Use Committee of the Meta-inflammation Research Center (permit number JWP-21-010). All surgery was performed under sodium pentobarbital anesthesia, and all efforts were made to minimize suffering.

2.3 Cortical Cerebral Blood Flow Measurement

Real-time two-dimensional cerebral blood flow (CBF) was monitored using a laser speckle contrast imager (PeriCam PSI HR System, Perimed, Sweden). Animal was inhalational

anesthetized with 1.5% isoflurane (volume-to-volume, v/v), mice were placed in the prone position and the skull was exposed through a cut in the skin at the parietal midline. A scanning camera was placed above the head at a working distance of 10 cm from the skull surface and illuminated with a laser diode (785 nm) to penetrate through the brain. To evaluate CBF changes, the region-of-interest (ROI) included the cortical area supplied by the middle cerebral artery.

2.4 *In vivo* Matrigel plug assays

This assay was performed by modification of methods previously described [32]. Mice were injected subcutaneously with 0.5 ml Matrigel (BD Biosciences) containing 100 ng recombinant murine VEGF (R&D Systems). Controls did not contain VEGF. After 10 days, the mice were sacrificed and plugs were harvested from underneath the skin. The plugs were fixed, embedded, and sectioned. To visualize capillaries, samples were immunohistochemically stained with anti-CD31 antibody (sc-376764, Santa Cruz).

2.5 Aortic ring assay

Aortas were prepared from wild-type and DRG2 KO mice, and aortic ring assays were performed by modification of methods previously described [33]. Briefly, 0.5 mm mouse aortic rings were embedded in 3-dimensional growth factor reduced Matrigel (354230, BD Biosciences). Opti-MEM (31985062, Thermo Fisher Scientific) containing 30 ng/mL VEGF (recombinant Murine VEGF165, #450-32, PeproTech) was added to induce vessel outgrowth. Vascular sproutings were counted every day for a period of 7 days, at which time they were photographed using a Nikon Eclipse TS 100 (Nikon) phase-contrast microscope.

2.6 Immunohistochemistry and quantification of lung angiogenesis

Immunohistochemical analysis was performed on 4 μm thick tissue sections cut from formalin-fixed paraffin-embedded surgical specimens. The sections were stained with hematoxylin and eosin (HE) or subjected to staining with anti-CD31 antibody (1:200 dilution; DAKO, Glostrup, Denmark) using a VENTANA BenchMark XT automated staining device (Ventana Medical System, Tucson AZ), according to the manufacturer's instructions. Vessel area was determined by CD31 positive staining normalized to total area fraction. Number of microvessels was counted as described previously [34]. Briefly, the most vascular areas were selected, and were counted on a x400 field. Any single or cluster of endothelial cells that was clearly separated from adjacent microvessels was considered as one countable microvessels. The average counts from the three most vascular areas were recorded for each case to measure the degree of angiogenesis.

2.7 Endothelial tube formation *in vitro* assays

The *in vitro* angiogenic activity of mLECs derived from wild-type and DRG2 KO mice was determined by matrigel tube formation assay. Matrigel (354230, BD Bioscience, San Jose, CA, USA) was added to each well (50 μL per well) of a 96-well plate and allowed to solidify at 37 °C for 30 min. Then, 1×10^4 mLEC cells in 100 μL of DMEM were placed in each well and incubated at 37 °C for 6 h with or without the addition of 100 ng/mL of mouse recombinant VEGF (BD Biosciences). The ability of the cells to form endothelial tubes was evaluated under phase-contrast microscopy using a Nikon Eclipse TS100 inverted microscope equipped with a Nikon DXM-1200 digital camera (Nikon, Tokyo, Japan). Images of tube morphology were taken in 5 random microscopic fields per sample at × 40 magnification, and the cumulative tube lengths were measured by Image-Pro Plus software

(Media Cybernetics, Rockville, MD, USA). Total tube length per well was determined by computer-assisted image analysis using the Image-Pro Plus program.

2.8 Colony forming assay

Clonogenic assays were carried out as described previously [35]. Briefly, 1600 cells were seeded into 60 mm plate and incubate for 2 h at 37 °C. Cell were further incubated for 2 weeks with or without the addition of 8 μM or 16 μM doxorubicin (Sigma). Cells were fixed with 3.7% formalin for 10 min and stained with 0.1 % crystal violet for 20 min. After washing in water, the colonies were counted.

2.9 Cell cycle analysis

Cells were harvested with Trypsin-EDTA (Gibco) and fixed for 30 min in ice-cold 70% ethanol. After washing twice with PBS, cells were incubated for 30 min at 37 °C with 100 μg/mL RNase (R5125, Sigma). A final concentration of 50 μg/ml of propidium iodide (PI) (P4170, Sigma) was added and DNA was measured with a flow cytometer (BD FACSCanto II, BD Biosciences).

2.10 Ki-67 analysis

Cells were fixed in 4% paraformaldehyde for 10 min and permeabilized with 0.5% Triton X-100 for 10 min. They were then incubated with Alexa Fluor 488-conjugated anti-Ki67 antibody (#11882, Cell Signaling) for 1 h. Fluorescence was analyzed using a FACSCanto II Flow Cytometer (BD Biosciences). Confocal images were obtained using an Olympus 1000/1200 laser-scanning confocal system (Olympus, Shinjuku, Japan). All images were

saved as TIFF files, and their contrast was adjusted with Image J (NIH, Bethesda, MD, USA, v1.19m). Quantification was performed by counting the number of Ki-67-positive cells.

2.11 MTS Assay

MTS assay was performed using the CellTiter 96 Aqueous One Solution Cell Proliferation Assay Kit (3580, Promega, Madison, WI, USA). Briefly, cells were plated in triplicate at 1×10^4 mLEC cells/well in 96-well culture plates in DMEM. At 24 h after plating, cell viability was measured using the MTS assay, according to the protocol supplied by the manufacturer.

2.12 Annexin-V staining

Apoptotic cells were stained using an Annexin-V-FLUOS staining kit (#6592, Cell Signaling), according to the protocol supplied by the manufacturer. Annexin-V-stained cells were analyzed for fluorescence intensity using a FACSCanto II Flow Cytometer (BD Biosciences).

2.13 Senescence-associated β-galactosidase (β-gal) activity

Senescence associated β-galactosidase activity was measured using the Senescence Cells Histochemical Kit (CS0030, Sigma) according to the protocol supplied by the manufacturer. Briefly, cells were incubated for 24 h with or without the addition of 200, 400, and 800 μM H_2O_2 (H1009-100ML, Sigma) or 5 mM N-Acetyl-Cysteine (NAC) (A9165-25G, Sigma) and, after fixation with Fixation buffer (2% formaldehyde and 0.2% glutaraldehyde) for 6 min, stained with Staining Mixture at 37 °C overnight. Cells were examined under ZEISS Primovert microscope (ZEISS, Germany) with ZEISS Axiocam ERc 5s camera (ZEISS, Germany). Senescence cells show blue staining in the cytosol.

To determine the SA-β-gal activity in uteruses, uteruses were collected from mice, fixed with 10% formaldehyde (v/v) (F1635, Sigma) for 10 min at room temperature, and incubated with a Staining mixture for 24 h at 37 ºC.

2.14 Confocal microscopy

Cells were seeded on 35-mm-diameter confocal dishes (200350, SPL). For detection of mitochondrial membrane potential, cells were labelled with 250 nM Tetramethylrhodamine, Methyl Ester, Perchlorate (TMRM, T668, Molecular Probes) in DMEM for 30 min. Nuclei were stained using 40,6-diamidino- 2-phenylindole (DAPI) (Sigma-Aldrich). Confocal images were obtained using an Olympus 1000/1200 laser-scanning confocal system (Olympus, Shinjuku, Japan) equipped with a 100x Plan Apochromat NA/1.4 oil objective and the appropriate filter combination. All images were saved as TIFF files, and their contrast was adjusted with IMAGE J (NIH, Bethesda, MD, USA, v1.19m). Images were analyzed with METAMORPH 7 software (Molecular Devices, San Jose, CA, USA, Universal Imaging) and IMARIS BITPLANE-7.7.2 (Oxford Instruments, Abingdon, UK) at the UNIST-Bio-imaging Center.

2.15 SDS-PAGE analysis and immunoblotting

Proteins were resolved by SDS-PAGE and transferred onto nitrocellulose membranes (10600001, GE Healthcare). The membranes were then probed with the appropriate dilutions of anti-DRG2 (#14743-1-AP, Proteintech), anti-β-actin (A5441, Sigma), anti-p53 (DO-1) (sc-126, Santa Cruz), anti-phosphpo-p53 (Ser15) (#9284), anti-caspase-3 (#9662), anti-PARP (46D11) (#9532), anti-phospho-histone H2A.X (Ser139) (#2577), anti-p38 MAPK (#9212),

anti-phospho-p38 MAPK (Thr180/Tyr182) (#9211), anti-p21 Waf1/Cip1 (DCS60) (#2946), anti-α-Tubulin (#2144, Cell Signaling). Immunoreactivity was detected using Amersham™ ECL™ Prime (RPN2232, Cytiva). Membranes were exposed at multiple time points to ensure that the images were not saturated. If required, the band densities were analyzed with NIH image software and normalized by comparison with the densities of internal control β-actin bands.

2.16 Quantitative real-time PCR and semi-qRT-PCR

Total RNA was extracted from cells using TRIzol (Thermo Fisher Scientific). Two micrograms of total RNA were reverse transcribed using oligo-dT (79237, Qiagen) and MMLV reverse transcriptase (3201, Beamsbio) according to the manufacturers' instructions. qRT-PCR was performed by monitoring the real-time increase in fluorescence of SYBR Green (MasterMix-R, Abm) using a StepOnePlus™ Real-Time PCR system (Applied Biosystems). RT-PCR was performed using Taq polymerase 2X premix (Solgent, Daejeon, Korea) and the appropriate primers. PCR primer pairs were as follows: IL-6, 5'-TAGTCCTTCCTACCCCAATTTCC-3' and 5'-TTGGTCCTTAGCCACTCCTTC-3' ; VEGF-A, 5'-AGGCTGCTGTAACGATGAA-3' and 5'-TATGTGCTGGCTTTGGTGAG-3' ; Catalase, 5'-GGAGGCGGGAACCCAATAG-3' and 5'-GTGTGCCATCTCGTCAGTGAA-3' ; GPX1, 5'-GTGCAATCAGTTCGGACACCA-3' and 5'-CACCAGGTCGGACGTACTTG-3' ; SOD1, 5'-TATGGGGACAATACACAAGGCT-3' and 5'-CGGGCCACCATGTTTCTTAGA-3' ; SOD2, 5'-TGGACAAACCTGAGCCCTAAG-3' and 5'-CCCAAAGTCACGCTTGATAGC-3' ; ARG1, 5'-ACAGAACTAAGCAAACGCC-3' and 5'-TTCATACCAGAAAGGAACTGC-3' ; ARG2, 5'-GGCTGAAGTGGTTAGTAGAG-3' and 5'-GGGCGTGACCGATAATG-3' ;

iNOS, 5’-GTTCTCAGCCCAACAATACAAGA-3’ and 5’-GTGGACGGGTCGATGTCAC-3’ ; eNOS, 5’-TCAGCCATCACAGTGTTCCC-3’ and 5’-ATAGCCCGCATAGCGTATCAG-3’ ; DRG2, 5’-CTCAACAGTCACACTGACAC-3’ , 5’-TACCGCAACTGATAACTACA-3’ ; GAPDH, 5’- ACATCAAGAAGGTGGTGAAG-3’ and 5’-CTGTTGCTGTAGCCAAATTC-3’ ; IFN-β1: 5’-AAAGCAAGAGGAAAGATTGACG-3’ and 5’-ACCACCATCCAGGCGTA-3’ ; CXCL10, 5’-CCAAGTGCTGCCGTCATTTTC-3’ and 5’-GGCTCGCAGGGATGATTTCAA-3’ ; RPLP0, 5’-AGATTCGGGATATGCTGTTGGC-3’ and 5’-TCGGGTCCTAGACCAGTGTTC-3’.

2.17 Measurement of NO production

Intracellular nitric oxide (NO) was measured using 4-Amino-5-Methylamino-2',7'-Difluorofluorescein Diacetate (DAF-FM diacetate) (D23844, Invitrogen). Cells were incubated in the dark with 10 μM DAF-FM diacetate for 60 min followed by washing twice with media. Nuclei were stained using 40,6-diamidino- 2-phenylindole (DAPI) (Sigma-Aldrich). Fluorescence was analyzed using a FACSCanto II Flow Cytometer (BD Biosciences) and an Olympus 1000/1200 laser-scanning confocal system (Olympus, Shinjuku, Japan).

2.18 Measurement of ROS levels

H_2O_2 levels were measured using the ROS-Glo™ H_2O_2 Assay (G8820, Promega) according to the protocol supplied by the manufacturer. Briefly, 1 x 10^4 cells/well were seeded in white

96 well plates and incubated for 24 h. After further incubation for 24 h with or without the addition of 8 μM or 16 μM doxorubicin (Sigma), the cells were incubated with 20 μL H_2O_2 substrate solution for 6 hours and with 100 μL of ROS-Glo™ Detection Solution for 20 min. Luminescence signal was measured using a SpectraMax L microplate reader (Molecular Devices).

2.19 Statistics analysis

For statistical comparisons, *P* values were determined using Student's *t*-test, one-way or two-way ANOVA. A *P* value < 0.05 was considered to indicate statistical significance.

III. RESULTS

3.1 DRG2$^{-/-}$ mice exhibit decreased microvascular circulation and blood vessel density

We previously demonstrated that DRG2 depletion in cancer cells suppress tumor angiogenesis [30]. In the current study, we further investigated the effects of DRG2 depletion on the endothelial cells behavior in the mouse. As a functional parameter, we determine whether DRG2 deficiency affects the microvascular circulation by evaluating the blood flow velocity of the cerebral cortex of wild-type and *DRG2*$^{-/-}$ mice under normal condition using laser speckle flowmetry. The results showed that the cerebral blood flow (CBF) of the ipsilateral cortex of *DRG2*$^{-/-}$ mice decreased to 72% of that of wild-type mice (Fig. 1A). The time course of the relative changes in CBF for vascular compartments are shown in Fig 1B. No significant changes in CBF levels of both wild-type and *DRG2*$^{-/-}$ mice were detected over the observing periods (Fig. 1B), which suggests that microvascular circulation of both wild-type and *DRG2*$^{-/-}$ mice was stabilized. The CBF levels of *DRG2*$^{-/-}$ mice were significantly lower than those of wild-type mice over the observing periods (20 sec) (Fig. 1B). We next determined whether DRG2 deficiency affects the blood vessel density in lung tissues. The sections of lung tissues from wild-type and *DRG2*$^{-/-}$ mice were stained for CD31, the marker of vascular endothelial cell. A representative lung section stained with anti-CD31 antibody is shown in Figure 1C and 1D, with quantitation for vessel area and microvessel number. Immunohistological analysis confirmed significantly reduced blood vessel density, measured as reduced percentage in CD31-positive vessel area (Fig. 1C), as well as a reduction in microvessel number (Fig. 1D) in the lung of *DRG2*$^{-/-}$ mice compared with that of wild-type mice. All these results showed that DRG2 deficiency decreases microvascular circulation and blood vessel density in mouse.

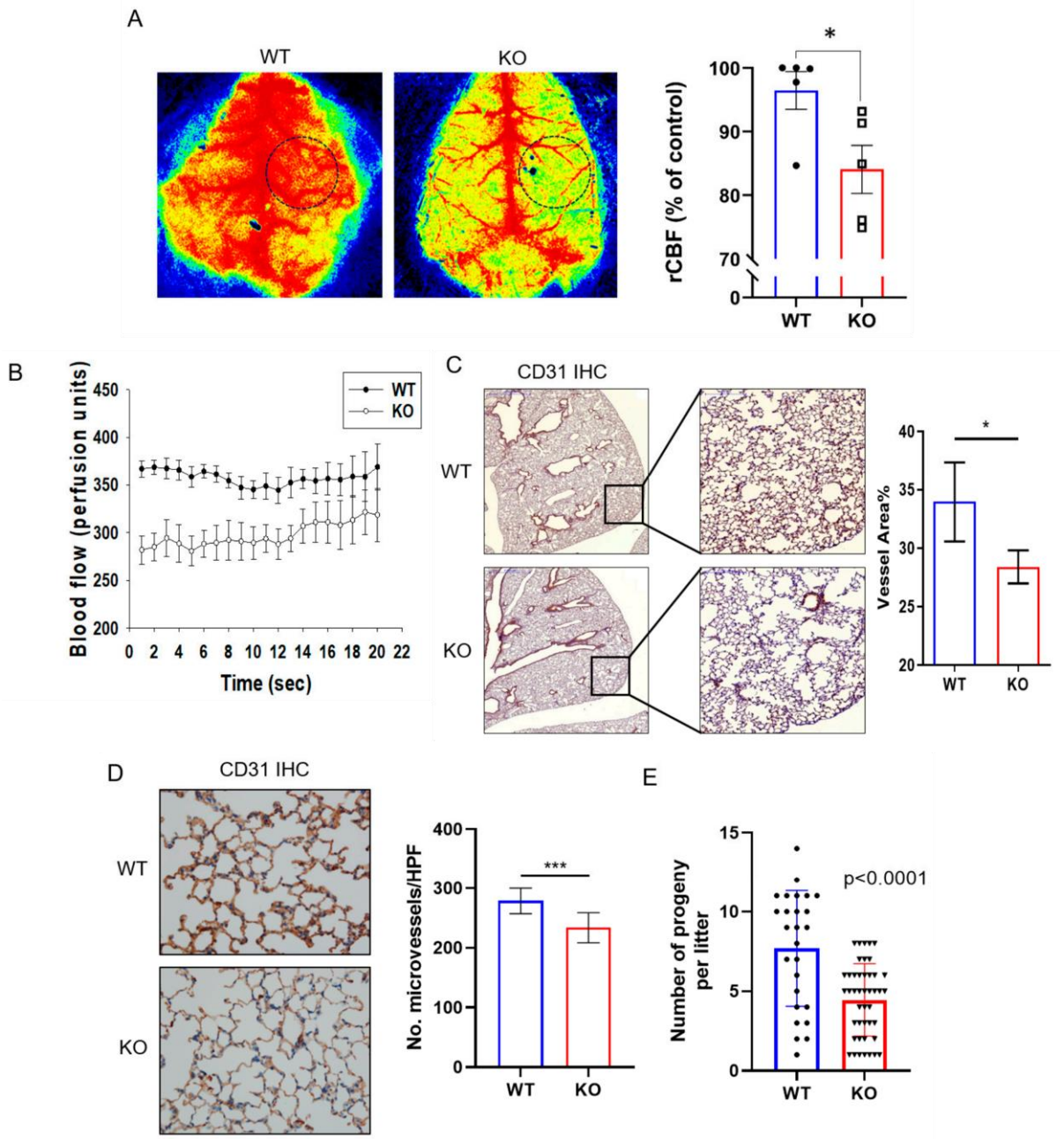

Figure 1. Effects of DRG2 deficiency on cerebral blood flow (CBF) and lung blood vessels density

(A, B) Effect of DRG2 deficiency on the CBF. (A) Representative laser speckle images of cerebral blood perfusion in wild-type (WT) and *DRG2*$^{-/-}$ (KO) mice. All images show areas of high and low blood perfusion as yellow–red and blue-black, respectively. CBF in the cerebral cortical area was calculated from the circular region-of-interest (ROI) (black dotted

line) and quantified (n=5 mice/group). *, $p < 0.05$. (B) The time courses changes in CBF at the circular ROI of the cerebral cortical area (n=5 mice/group). (C & D) Effect of DRG2 deficiency on blood vessel density of mouse lung. (C) Representative microscopic images of CD31 immunohistochemistry of mouse lungs (original magnification, 10x and 40x, respectively) with quantification of vessel area fraction. The data are expressed as the mean ± SEM (n = 15 in each group). *, $p < 0.05$. (D) Representative microscopic images from hot spot areas of mouse lung immunostained for CD31 (original magnification, 400x) with quantification of microvessel number per HPF. The data are expressed as the mean ± SEM (n = 15 in each group). ***, $p < 0.001$. (E) Quantification of the number of progeny per litter of wild-type and DRG2$^{-/-}$. The data are expressed as mean ± SD. (n = 26 for wildtype and 45 for DRG2$^{-/-}$).

3.2 *DRG2 deficiency inhibits angiogenic functions of endothelial cells*

The endothelial cells lining all of blood vessels are critically involved in many physiological functions of blood vessels [36]. To determine the effect of DRG2 deficiency on angiogenic function of endothelial cells, three studies were conducted. Firstly, we investigated influence of DRG2 deficiency on the formation of capillary-like tubes by primary lung endothelial cells (mLEC) after addition of recombinant VEGF-A. VEGF-A was found to stimulate tube formation by both wild-type and *DRG2*$^{-/-}$ mLECs (Fig. 2A & 2B). However, the total tube lengths in *DRG2*$^{-/-}$ mLECs treated with 100 ng/ml VEGF-A was significantly decreased compared with those of wild-type mLECs (Fig. 2A & 2B), demonstrating that DRG2 deficiency impaired endothelial cell tube formation *in vitro*.

Secondly, we assessed the effect of DRG2 deficiency on angiogenic potential of mice, by *in vivo* Matrigel plug assay. Matrigel was subcutaneously injected into the wild-type and *DRG2*$^{-/-}$ mice, and the implants were removed after 10 days to evaluate neovascularization. To allow efficient vascularization, angiogenic growth factor VEGF-A was suspended in the Matrigel prior to injection. Controls did not contain VEGF-A supplement. The plug in red color abundantly filled with red blood cells (RBCs) indicated the formation of new blood vessels inside the matrigel. As shown in Figure 2C, the red color of plugs from *DRG2*$^{-/-}$ mice was much lighter than those from wild-type mice, suggesting the formation of fewer blood vessels in *DRG2*$^{-/-}$ mice. Matrigel plugs were harvested, sectioned, and the presence of capillaries in the matrigel was further detected by immunohistochemical (IHC) staining with anti-CD31 antibody. The overall vascular densities in Matrigel plugs are shown in Figure 2D. *DRG2*$^{-/-}$ mice exhibited lower neovascularization of the Matrigel implants upon angiogenic challenge with VEGF compared with wild-type mice (Fig. 2D). Without the addition of

VEGF-A (i.e., controls), the implants remained largely avascular. In addition, while an orderly vascular endothelial structure was detected in the plugs from wild-type mice, the blood vessels in the plugs from *DRG2*$^{-/-}$ mice were poorly organized (Fig. 2D).

Thirdly, we prepared aortas from wild-type and *DRG2*$^{-/-}$ mice and determined the effect of DRG2 deficiency on endothelial cell outgrowth by performing aortic ring assay. Results from the aortic ring assays, analyzing the newly formed endothelial cell network protruding from aortic explants, are compared in Figure 2E. Endothelial cell tubes protruding from aortic explants of *DRG2*$^{-/-}$ mice formed a less complex endothelial network compared with the rather dense network emerging from explants of wild-type mice. In addition, the overall length of the endothelial cell sprouts emerging from the aortic explants of DRG2−/− mice was significantly lower than that of wild-type mice (Figure 2F). Collectively, these results suggest that DRG2 deficiency leads to defective angiogenesis.

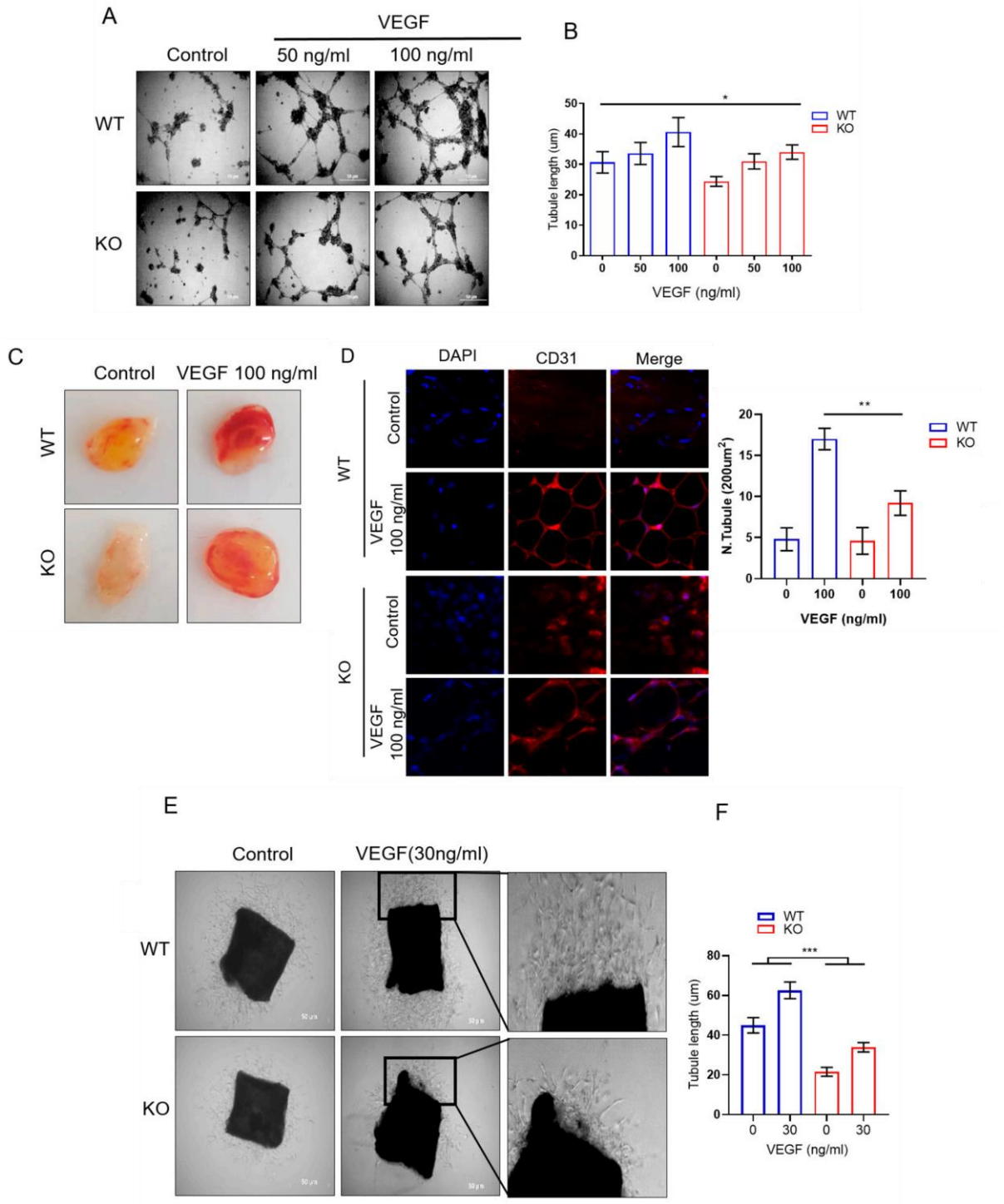

Figure 2. Effects of DRG2 deficiency on angiogenic function of endothelial cells

(A & B) Effects of DRG2 deficiency on tube formation of mouse lung endothelial cells (mLECs). mLECs from WT and *DRG2*$^{-/-}$ (KO) mice seeded on Matrigel were monitored for

tube formation after incubation of 24 h in the absence or presence of recombinant VEGF-A (50 or 100 ng/ml). (A) Representative images of tube formation by MLEC cells stimulated with recombinant VEGF-A or the supernatant of melanoma cells. Scale bar = 50 μm. (B) Quantification of the length of tubes. Data represent the tube length from four randomly chosen fields of three independent experiments and mean ± SD. Two-way ANOVA, $*P < 0.05$. (C & D) Effect of DRG2 deficiency on the neovascularization in the Matrigel plug. Wild-type and *DRG2*$^{-/-}$ (KO) mice were s.c. injected with Matrigel plugs containing 100 ng/ml VEGF and blood vessels were developed for 10 days. (C) Representative macroscopic images of Matrigel plugs from wild-type and *DRG2*$^{-/-}$ mice. (D) Representative images of anti-CD31 stained paraffin sections of Matrigel plugs from wild-type and *DRG2*$^{-/-}$ mice CD31 (original magnification, 400x) with quantification of CD31-positive vessels. A total of 3 fields from individual plugs of 3 animals per group were counted. The data are expressed as the mean ± SD (n = 9 in each group). **, $p < 0.005$. (E,F) Effect of DRG2 deficiency on the endothelial cell sprouting in an aorta ring assay. Aortic rings obtained from wild-type and *DRG2*$^{-/-}$ mice were incubated for 7 days in the absence or presence of VEGF-A (30 ng/ml). (E) Representative areas of the aortic rings are marked with boxes and enlarged correspondingly on the right side of each panel (original magnification, 100x). (F) The graph represents the overall length of endothelial cell sprouts and the overall number of endothelial cell sprouts emerging from the aortic ring. The data are expressed as the mean ± SD (n = 6 aortic rings from two mice in each group). **, $p < 0.001$.

3.3 *DRG2 deficiency decreases EC proliferation and enhances EC senescence*

Cell proliferation is essential for endothelial cells to adequately perform their angiogenic functions and senescence of endothelial cells impairs angiogenesis [37]. The defects in angiogenic function of *DRG2*$^{-/-}$ endothelial cells prompted us to investigate whether DRG2 deficiency affects proliferation of endothelial cells. We first determined the effect of DRG2 deficiency on mLECs proliferation using MTS assay. *DRG2*$^{-/-}$ mLECs demonstrated decreased proliferation compared with that of *DRG2*$^{+/+}$ mLECs (Fig. 3A). The Ki67 staining study further supported decreased proliferation of *DRG2*$^{-/-}$ mLECs (Fig. 3B). Since apoptosis may contribute to the numbers of endothelial cells, we examined the apoptotic activity in mLECs by Annexin V staining. However, there was no significant difference in apoptosis between wild-type and *DRG2*$^{-/-}$ mLECs (Fig. 3C). We next asked whether DRG2 deficiency affects senescence of endothelial cells. We evaluated the senescence-associated β-gal (SA-β-gal) activity as a cellular senescence marker in wild-type and *DRG2*$^{-/-}$ mLECs. The number of SA-β-gal-stained cells was significantly increased in *DRG2*$^{-/-}$ mLECs compared with that of *DRG2*$^{+/+}$ mLECs (Fig. 3D). These results indicate that DRG2 deficiency decreases proliferation and increases senescence of endothelial cells.

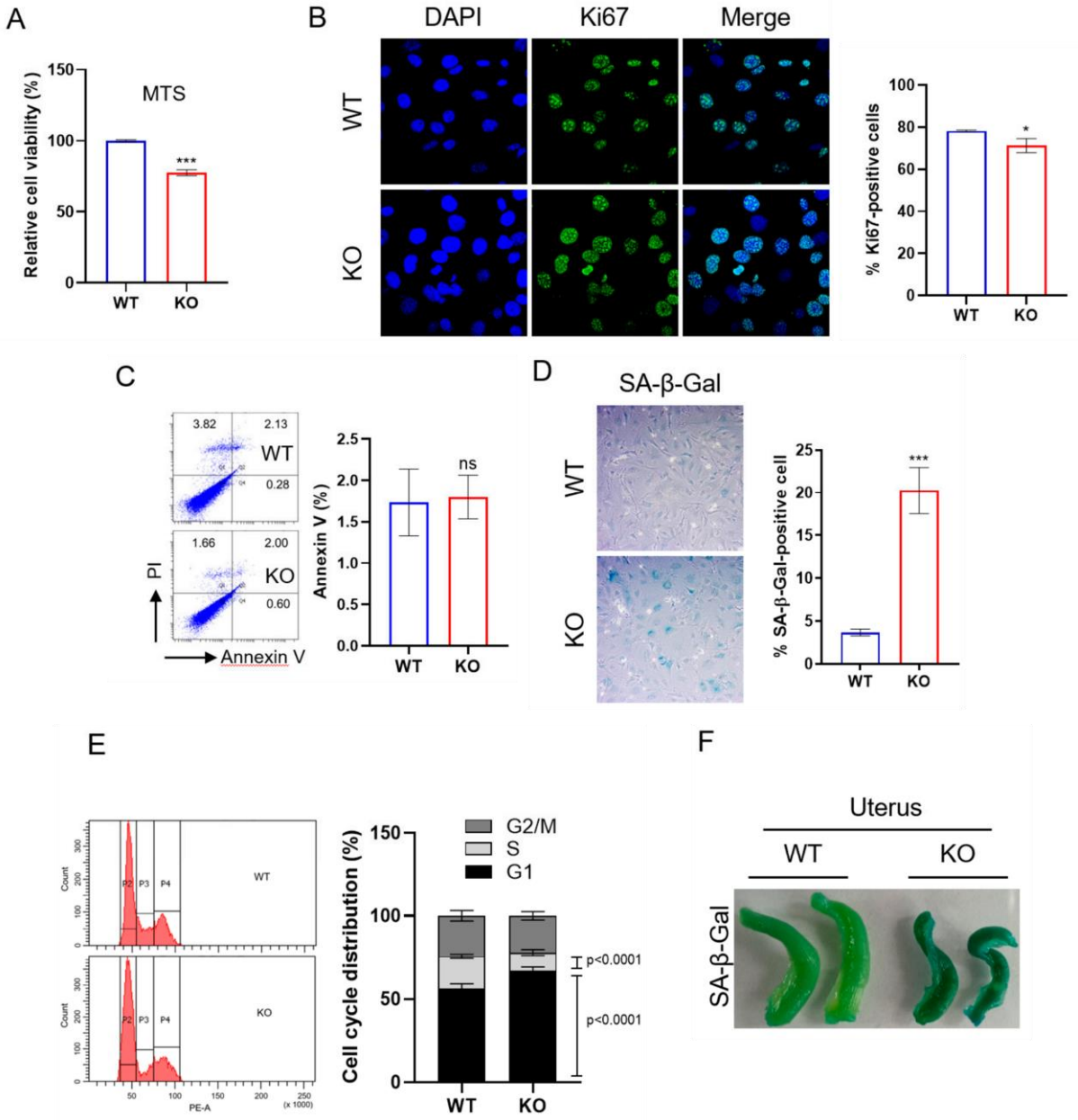

Figure 3. Effect of DRG2 deficiency on the proliferation, apoptosis, and senescence of endothelial cells

Lung endothelial cells (mLECs) derived from wild-type and *DRG2*$^{-/-}$ mice were cultivated under normal condition as described in the **Materials and Methods** section without any treatment. The mLECs were analyzed by (A) MTS assay (n=3 independent experiments in each group) and (B) Ki67 staining for cell proliferation (n = 40 cells per 3 independent experiments in each group), (C) Annexin-V staining for apoptosis (n=3 independent

experiments in each group), (D) senescence-associated β-gal (SA-β-gal) staining for cellular senescence (n=120 cells per 3 samples independent experiments in each group), and (E) FACS analysis for cell cycles arrest (n=10 independent experiment). (F) Detection of SA-β-gal activity in uteruses from wild-type and DRG2$^{-/-}$ mice. Images in (B) and (D) are representative ones (600x and 200x magnification, respectively) of Ki67-stained cells and SA-β-gal-stained cells, respectively. The data are expressed as the mean ± SD. *, $p < 0.05$; **, $p < 0.005$; ***, $p < 0.001$. ns, not significant

3.4 DRG2 deficiency enhances DNA damage and senescence induced by oxidative stress

Oxidative stress causes DNA damage [38] and cellular senescence [39], [40]. Since H_2O_2 is a major reactive oxygen species generated during oxidative stress [41], [42], we next examined whether DRG2 deficiency affect the senescence response to oxidative stress using H_2O_2. Treatment of H_2O_2 significantly increased the number of SA-β-gal-stained cells in both wild-type and *DRG2*$^{-/-}$ mLECs (Fig. 4A). However, after H_2O_2 treatment, number of SA-β-gal-stained cells in *DRG2*$^{-/-}$ mLECs was much higher than that of wild-type mLECs (Fig. 4A). Accumulated DNA damage activates p53, leading to cellular senescence (Ou and Schumacher, 2018). An increase in phosphorylated histone H2AX (γH2AX) has been considered as a biomarker of celluler senescence [43]. We examined the effect of DRG2 deficiency on the oxidative stress-induced DNA damage by analyzing the levels of phosphorylated p53 and γH2AX. After H_2O_2 treatment, *DRG2*$^{-/-}$ mLECs showed significantly higher level of total and phosphorylated p53 than wild-type mLECs (Fig. 4B). Consistently, the level of γH2AX induced by H_2O_2 was higher in *DRG2*$^{-/-}$ mLECs than that in WT mLECs (Fig. 4C). Even in the absence of H_2O_2 treatment, *DRG2*$^{-/-}$ mLECs showed higher level of phosphorylated p53 and γH2AX than WT mLECs (Fig. 4B & 4C). We also treated cells mLECs with DNA damaging agents, doxorubicin and etoposide, and analyzed the expression levels of phosphorylated p53. Consistent with H_2O_2, *DRG2*$^{-/-}$ mLECs showed significantly higher level of phosphorylated p53 than wild-type mLECs after treatment with doxorubicin (Fig. 4D) and etoposide (Fig. 4E). In addition, doxorubicin and etoposide induced higher level of p21 in *DRG2*$^{-/-}$ mLECs than wild-type mLECs (Fig. 4D & 4E). Senescent cells are characterized by production of inflammatory cytokines, immune modulators, growth factors, and proteases, which comprise the senescence-associated secretory phenotype (SASP) [44]. To determine if DRG2 deficiency

would also induce components of the SASP, levels of IL-6, CXCL10, and IFN-β1 in wild-type and *DRG2*$^{-/-}$ mLECs were measured after etoposide using qPCR. After etoposide treatment, *DRG2*$^{-/-}$ mLECs expressed significantly higher levels of these cytokines than wild-type mLECs (Fig. 4F). These data suggest that *DRG2*$^{-/-}$ mLECs show enhanced DNA damage and cellular senescence by oxidative stress.

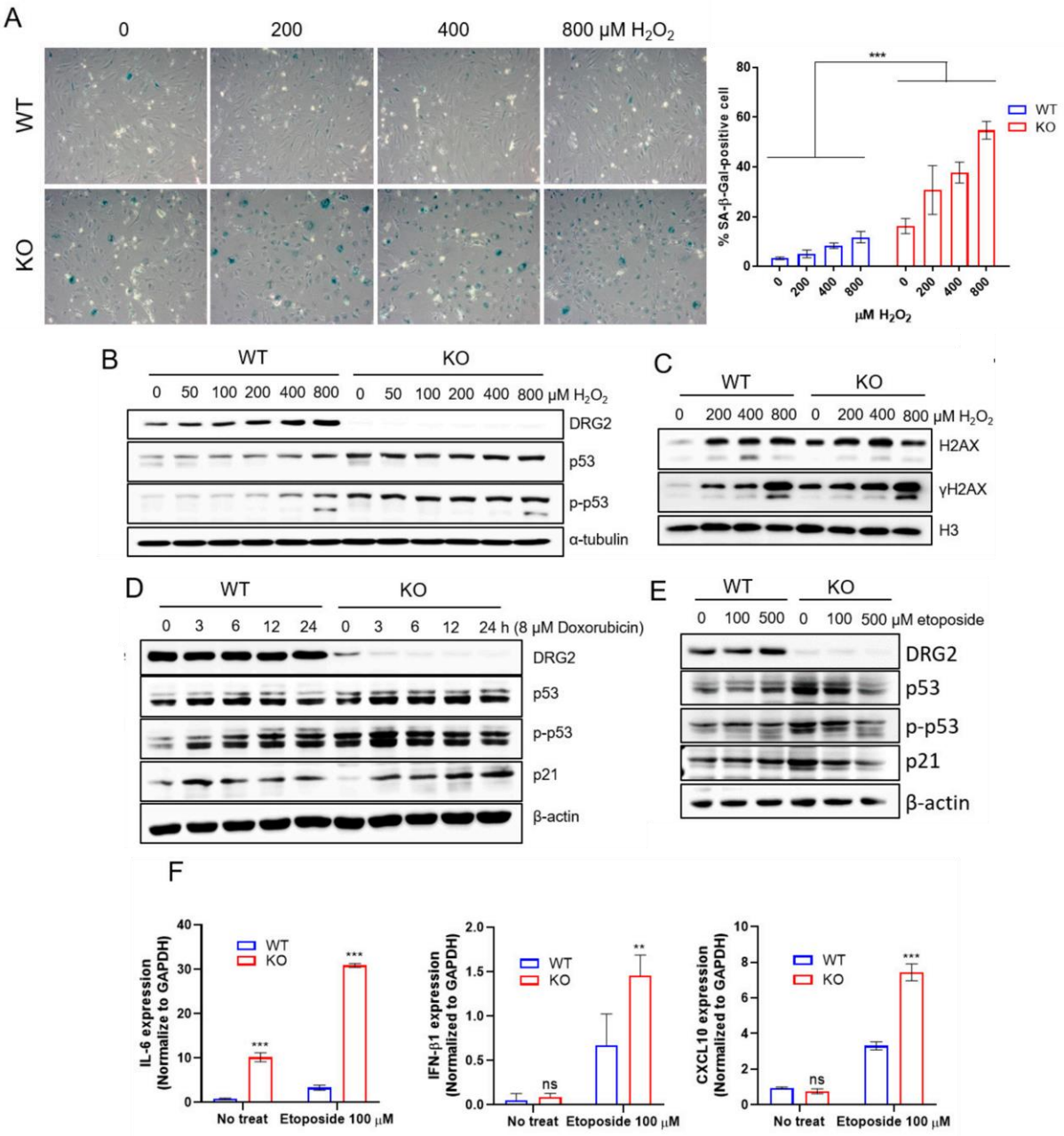

Figure 4. Effect of DRG2 deficiency on oxidative stress-induced senescence of endothelial cells

(A-C) mLECs from wild-type and *DRG2*$^{-/-}$ mice were exposed to H_2O_2 at the indicated concentrations for 6 h. (A) Representative images of SA-β-gal-stained cells (200x magnification) with quantification of SA-β-gal-positive cells. The data are expressed as the mean ± SD (n = 5 in each group). ***, $p < 0.001$. (B, C) Cells were analyzed by Western blot assay for the levels of (B) total and phosphorylated p53, and (C) γH2AX. (D) mLECs from

wild-type and *DRG2*$^{-/-}$ mice were treated with 8 μM doxorubicin for the indicated time and analyzed by Western blot assay for the levels of total and phosphorylated p53, and p21. (E) mLECs from wild-type and *DRG2*$^{-/-}$ mice were treated with indicated concentration of etoposide for 24 h and analyzed by Western blot assay for the levels of total and phosphorylated p53, and p21. All Western blot data were representative ones of more than two experiments. (F) mLECs from wild-type and *DRG2*$^{-/-}$ mice were incubated for 6 h in the absence or presence of 100 μM etoposide and analyzed by qPCR for the levels of IL-6, IFN-β1 and CXCL10. The data are expressed as the mean ± SD (n = 3 in each group). **, $p < 0.005$.***, $p < 0.001$.

3.5 DRG2 deficiency affect the expression of antioxidant genes

Previously, we have reported that DRG2 deficiency induces mitochondrial dysfunction and increases intracellular ROS in cancer cells [28, p. 1]. Consistently, DRG2−/− mLECs showed a decrease in mitochondrial membrane potential compared with wild-type mLECs (Figure 5A). We also confirmed an increase in intracellular ROS level before and after doxorubicin treatment in *DRG2*$^{-/-}$ mLECs compared to wild-type mLECs (Fig. 5B). Since oxidative stress is one of the major factors causing the onset of senescence [39], we used ROS scavenger N-acetylcysteine (NAC) to test whether increased ROS level leads to increase in senescence in *DRG2*$^{-/-}$ mLECs. NAC treatment effectively reduced the number of SA-β-gal-stained cells in both wild-type and *DRG2*$^{-/-}$ mLECs (Fig. 5C), indicating that increased ROS is one of the major causative factor for induction of senescence in mLECs. To combat oxidative stress, cells produce several antioxidant enzymes [45]. We next examined whether DRG2 deficiency affects the expression of antioxidant genes, superoxide dismutase 1 (SOD1) and SOD2. The expression levels of SOD1 (Fig. 5D) and SOD2 (Fig. 5E) were significantly lower in *DRG2*$^{-/-}$ mLECs both before and after H_2O_2 treatment compared to those than in wild-type mLECs, implicating that reduced expression of anti-oxidant genes may play a role in increased ROS level and senescence in *DRG2*$^{-/-}$ mLECs.

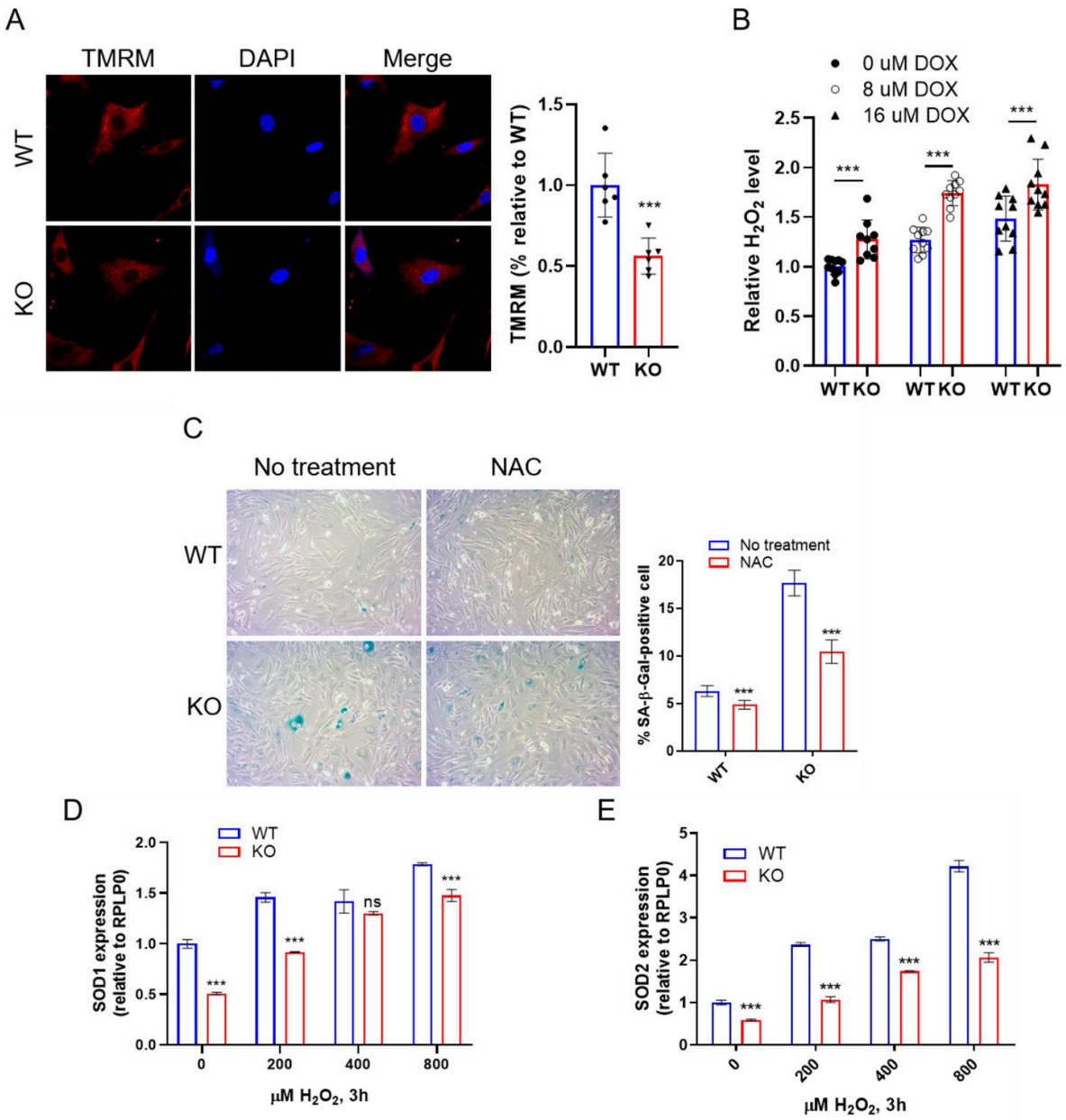

Figure 5. Effect of DRG2 deficiency on the production of reactive oxygen species (ROS) in endothelial cells

(A) Representative images of wild-type and DRG2$^{-/-}$ mLECs stained with TMRM for mitochondrial membrane potential and DAPI for nucleus (original magnification 600×). The data are expressed as the mean ± SD (n = 6 in each group). *** $p < 0.001$. (B) mLECs from wild-type and DRG2$^{-/-}$ mice were exposed to doxorubicin at the indicated concentrations for 6 h and were analyzed for H_2O_2 levels as described in the **Materials and Methods** section.

The level obtained from untreated wild-type mLECs was set to 1. The data are expressed as the mean ± SD (n = 10 in each group). *** $p < 0.001$. (C) Representative images of SA-β-gal-stained cells (original magnification 200×) with quantification of SA-β-gal-positive cells. mLECs from wild-type and DRG2$^{-/-}$ mice were exposed to 5 mM NAC for 6 h and were analyzed for SA-β-gal-positive cells. The data are expressed as the mean ± SD (n = 3 in each group). *** $p < 0.001$. (D–E) Effect of DRG2 deficiency on the H_2O_2 induced expression of anti-oxidant genes in endothelial cells. mLECs from wild-type and DRG2$^{-/-}$ mice were exposed to H_2O_2 at the indicated concentrations for 6 h and analyzed by qPCR for the levels of SOD1 and SOD2. The data are expressed as the mean ± SD (n = 3 in each group). ns, not significant. *** $p < 0.001$.

3.6 DRG2 deficiency decreases eNOS expression and NO production in endothelial cells

Since eNOS-derived NO functions as an anti-senescent factor in ECs [46], we examined the effect of DRG2 deficiency on the eNOS/NO pathway. There was no significant difference in the expression of eNOS between *DRG2*$^{-/-}$ mLECs and wild-type mLECs (Fig. 6A). However, NO production was significantly decreased in *DRG2*$^{-/-}$ mLECs compared to wild-type mLECs (Fig. 6B). Arg2 promoted eNOS uncoupling, decreased NO production, and increased ROS generation leading to endothelial dysfunction [47], [48]. We next examined whether DRG2 deficiency affects the expression of Arg2 in endothelial cells. The expression levels of Arg2 were significantly higher in *DRG2*$^{-/-}$ mLECs both before and after etoposide treatment than wild-type mLECs (Fig. 6C). Collectively, these results suggest that the senescence induction by DRG2 deficiency in mLECs is associated with modulation of expression of Arg2, which affect the intracellular levels of NO and ROS.

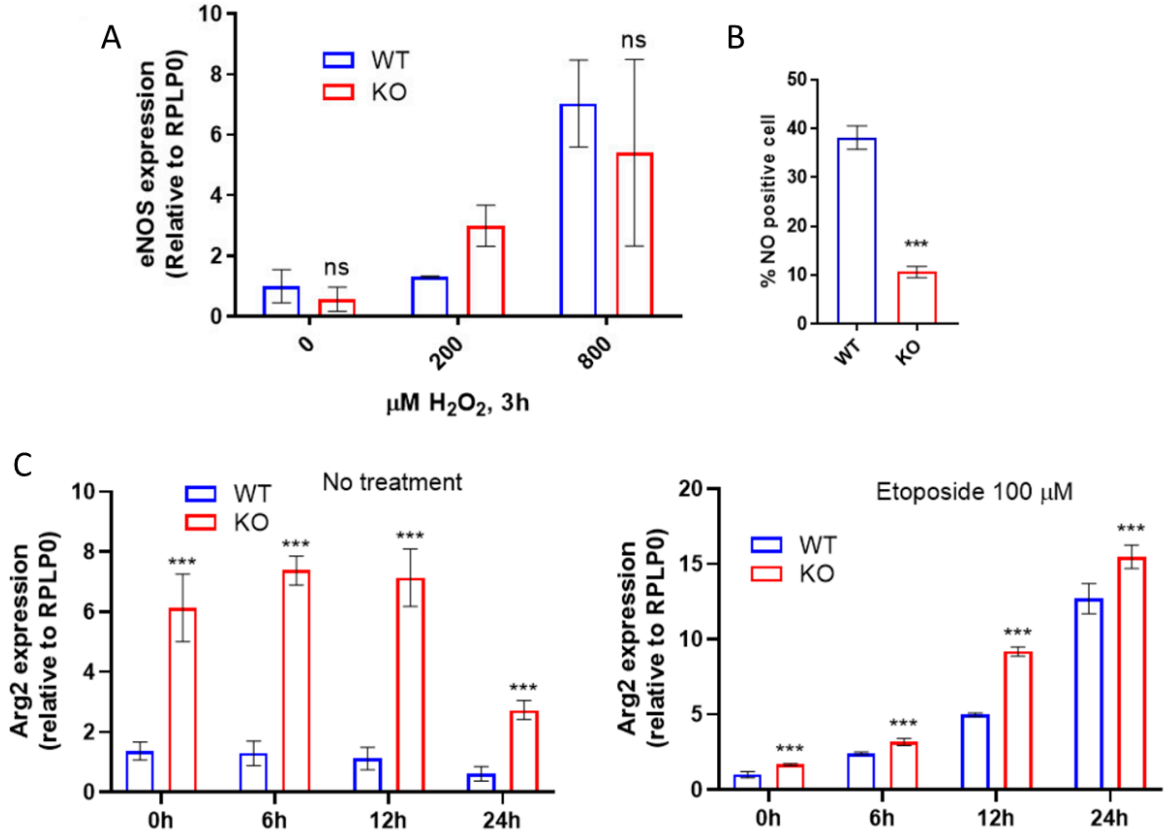

Figure 6. Effect of DRG2 deficiency on the production of NO in endothelial cells

(A) Effect of DRG2 deficiency on the H_2O_2 induced expression of anti-oxidant genes in endothelial cells. mLECs from wild-type and DRG2$^{-/-}$ mice were exposed to H_2O_2 at the indicated concentrations for 6 h and analyzed by qPCR for the levels of eNOS. The data are expressed as the mean ± SD (n = 3 in each group). ns, not significant. *** $p < 0.001$. (B) Effect of DRG2 deficiency on the production of nitric oxide (NO) in endothelial cells. mLECs from wild-type and DRG2$^{-/-}$ mice cultivated under normal condition without any treatment were analyzed for NO production as described in the **Materials and Methods** section. The data are expressed as the mean ± SD (n = 3 in each group). *** $p < 0.001$. (C) mLECs from wild-type and DRG2$^{-/-}$ mice were incubated in the absence or presence of 100 μM etoposide for the indicated time and analyzed by qPCR for level of Arginase 2 (Arg2).

The data are expressed as the mean ± SD (n = 3 in each group). *** $p < 0.001$.

IV. DISCUSSION

Our previous data suggested that DRG2 in cancer cells is involved in tumor angiogenesis [30]. However, the role of DRG2 in endothelial cells remain to be explored. In the present study, we investigated the role of DRG2 in endothelial cell functions, especially the angiogenic function, using *DRG2*$^{-/-}$ mice. We here provide evidences that DRG2 is involved in angiogenesis and vascular remodeling. (a) *DRG2*$^{-/-}$ mice showed decreased blood flow in brain. Since the regulation of cerebral blood flow is controlled by cerebral endothelium [49], reduction in the cerebral blood flow in *DRG2*$^{-/-}$ mice implicate the role of DRG2 in endothelium function. (b) DRG2 deficiency reduced the pulmonary blood vessel density. The staining intensity CD31 in lung of *DRG2*$^{-/-}$ mice was significantly reduced compared to that of wild-type mice. (c) DRG2 deficiency inhibited the neovascularization of subcutaneous Matrigel implants. When Matrigel plugs containing angiogenic growth factor VEGF were transplanted subcutaneously, *DRG2*$^{-/-}$ mice exhibited low and poorly organized neovascularization of the Matrigel implant compared to wild-type mice. These results suggest that DRG2 deficiency leads to defect in angiogenesis. (d) DRG2 deficiency impaired microvessel outgrowth in ex vivo aorta ring assay. In aortic ring assays, branching of newly formed sprouts was significantly reduced in *DRG2*$^{-/-}$ aorta explants compared to WT aorta explant. (e) DRG2 deficiency reduced in vitro tube-forming capability of endothelial cells. When treated with VEGF, lung endothelial cells from *DRG2*$^{-/-}$ mice showed decrease in formation of tube-like structures compared to those from wild-type mice. Collectively, our results suggest that DRG2 deficiency induces dysfunction of endothelial cells, especially defect in angiogenesis.

Cell proliferation is essential for endothelial cells to adequately perform their angiogenic

functions and senescence of endothelial cells may contribute to endothelial dysfunction and impair angiogenesis [37], [50]. We previously reported that DRG2 deficiency increases intracellular ROS level in cancer cells [28, p. 1]. Consistently, in this experiment, we also found that *DRG2*$^{-/-}$ endothelial cells produce enhanced level of ROS compared to wild-type endothelial cells. The ROS can induce DNA damage [38] and cellular senescence [39], [40]. In the present work, we found that DRG2 deficiency enhanced SA-β-gal activity, a biomarker for senescence [51], in endothelial cells. The increase of SA-β-gal activity in *DRG2*$^{-/-}$ endothelial cells was attenuated by concomitant application of NAC, a ROS scavenger, indicating that increased ROS level led to increased senescence in *DRG2*$^{-/-}$ endothelial cells. Characteristic feature of cellular senescence is the SASP [44] involving increased expression of inflammatory molecules [52]. In the present work, we also found that *DRG2*$^{-/-}$ endothelial cells expressed higher levels of inflammatory molecules such as IL-6, CXCL-10, and IFN-β1 than wild-type endothelial cells, thereby supporting the induction of senescence in *DRG2*$^{-/-}$ endothelial cells. The excessive ROS production can induce DNA damage [40], [53], [54] and activate p53-p21$^{WAF1/CIP1}$ senescence pathway [55], [56], [57]. Consistently, we here observed increased levels of DNA damage marker γH2AX [43], p21 and phosphorylated p53 in *DRG2*$^{-/-}$ endothelial cells compared to wild-type endothelial cells. Collectively, our results indicated that DRG2 deficiency increases intracellular ROS, which leads to DNA damage and senescence in endothelial cells.

How does DRG2 deficiency increase ROS in endothelial cells? Endothelial nitric oxide synthase (eNOS) plays a key role in increase of vascular ROS production [58]. eNOS is the predominant NOS form in the vasculature and normally oxidizes its substrate L-arginine to produce the vasoprotectant molecule NO [59]. However, under limited-L-arginine condition, eNOS produces ROS instead of NO, referred to as eNOS uncoupling [60], [61]. Endothelial

cells express arginases that can compete with eNOS for L-arginine and, if highly expressed, "starve" eNOS. Arginase exists in 2 isoforms; in human endothelial cells, Arg2 seems to be the predominant isozyme [15], [62]. Upregulation of Arg2 has been found to decrease NO generation and increase ROS production via eNOS uncoupling [48]. In the present work, we found that, even though DRG2 deficiency did not affect the eNOS expression, it down-regulated the intracellular NO level in endothelial cells. When we analyzed the expression level of Arg2, we found that *DRG2*$^{-/-}$ endothelial cells produced higher level of Arg2 than wild-type endothelial cells, suggesting the possibility that *DRG2*$^{-/-}$ endothelial cells produce ROS via eNOS uncoupling. Although our study did not determine other sources of ROS, our results suggest that eNOS uncoupling is an important contributor to ROS production and senescence induction in *DRG2*$^{-/-}$ endothelial cells.

In summary, we demonstrated that DRG2 deficiency induced endothelial dysfunction such as reduced blood flow and decrease in angiogenesis *in vivo*, *ex vivo*, and *in vitro*. DRG2 deficiency increased ROS production in endothelial cells through eNOS uncoupling and induced endothelial senescence. The enhanced endothelial senescence may contribute to the dysfunction found in DRG2-deficient endothelium. Even though we did not determine whether *DRG2*$^{-/-}$ mice showed enhanced frequency of vascular diseases, it is possible that DRG2 deficiency may increase ROS and thus endothelial dysfunction and lead to vascular diseases. Further studies are required to explore in more detail the roles of DRG2 in DNA damage, endothelial senescence, and vascular diseases.

REFERENCES

[1] J. E. Deanfield, J. P. Halcox, and T. J. Rabelink, “Endothelial function and dysfunction: testing and clinical relevance,” *Circulation*, vol. 115, no. 10, pp. 1285–1295, Mar. 2007, doi: 10.1161/CIRCULATIONAHA.106.652859.

[2] H. F. Galley and N. R. Webster, “Physiology of the endothelium,” *British Journal of Anaesthesia*, vol. 93, no. 1, pp. 105–113, Jul. 2004, doi: 10.1093/bja/aeh163.

[3] H. M. Eilken and R. H. Adams, “Dynamics of endothelial cell behavior in sprouting angiogenesis,” *Current Opinion in Cell Biology*, vol. 22, no. 5, pp. 617–625, Oct. 2010, doi: 10.1016/j.ceb.2010.08.010.

[4] P. Carmeliet, “Angiogenesis in health and disease,” *Nat Med*, vol. 9, no. 6, pp. 653–660, Jun. 2003, doi: 10.1038/nm0603-653.

[5] F. Rodier and J. Campisi, “Four faces of cellular senescence,” *Journal of Cell Biology*, vol. 192, no. 4, pp. 547–556, Feb. 2011, doi: 10.1083/jcb.201009094.

[6] T. Minamino and I. Komuro, “Vascular Cell Senescence,” *Circulation Research*, vol. 100, no. 1, pp. 15–26, Jan. 2007, doi: 10.1161/01.RES.0000256837.40544.4a.

[7] A. D. Leonardo, S. P. Linke, K. Clarkin, and G. M. Wahl, “DNA damage triggers a prolonged p53-dependent G1 arrest and long-term induction of Cip1 in normal human fibroblasts.,” *Genes Dev.*, vol. 8, no. 21, pp. 2540–2551, Nov. 1994, doi: 10.1101/gad.8.21.2540.

[8] C. M. Counter *et al.*, “Telomere shortening associated with chromosome instability is arrested in immortal cells which express telomerase activity,” *EMBO J*, vol. 11, no. 5, pp. 1921–1929, May 1992.

[9] R. Colavitti and T. Finkel, “Reactive Oxygen Species as Mediators of Cellular Senescence,” *IUBMB Life*, vol. 57, no. 4–5, pp. 277–281, 2005, doi: 10.1080/15216540500091890.

[10] P. Davalli, T. Mitic, A. Caporali, A. Lauriola, and D. D’Arca, “ROS, Cell Senescence, and Novel Molecular Mechanisms in Aging and Age-Related Diseases,” *Oxidative Medicine and Cellular Longevity*, vol. 2016, p. e3565127, May 2016, doi: 10.1155/2016/3565127.

[11] A. C. Cave *et al.*, “NADPH Oxidases in Cardiovascular Health and Disease,” *Antioxidants & Redox Signaling*, vol. 8, no. 5–6, pp. 691–728, May 2006, doi: 10.1089/ars.2006.8.691.

[12] M. Ushio-Fukai, “Redox signaling in angiogenesis: Role of NADPH oxidase,” *Cardiovascular Research*, vol. 71, no. 2, pp. 226–235, Jul. 2006, doi: 10.1016/j.cardiores.2006.04.015.

[13] Z. Ungvari, G. Kaley, R. de Cabo, W. E. Sonntag, and A. Csiszar, “Mechanisms of Vascular Aging: New Perspectives,” *The Journals of Gerontology: Series A*, vol. 65A, no. 10, pp. 1028–1041, Oct. 2010, doi: 10.1093/gerona/glq113.

[14]H. Li and U. Förstermann, “Nitric oxide in the pathogenesis of vascular disease,” *The Journal of Pathology*, vol. 190, no. 3, pp. 244–254, 2000, doi: 10.1002/(SICI)1096-9896(200002)190:3<244::AID-PATH575>3.0.CO;2-8.

[15] X.-F. Ming *et al.*, “Thrombin Stimulates Human Endothelial Arginase Enzymatic Activity via RhoA/ROCK Pathway,” *Circulation*, vol. 110, no. 24, pp. 3708–3714, Dec. 2004, doi: 10.1161/01.CIR.0000142867.26182.32.

[16] Y. C. Luiking, G. A. M. Ten Have, R. R. Wolfe, and N. E. P. Deutz, “Arginine de novo and nitric oxide production in disease states,” *American Journal of Physiology-Endocrinology and Metabolism*, vol. 303, no. 10, pp. E1177–E1189, Nov. 2012, doi: 10.1152/ajpendo.00284.2012.

[17] D. E. Berkowitz *et al.*, “Arginase Reciprocally Regulates Nitric Oxide Synthase Activity and Contributes to Endothelial Dysfunction in Aging Blood Vessels,” *Circulation*, vol. 108, no. 16, pp. 2000–2006, Oct. 2003, doi: 10.1161/01.CIR.0000092948.04444.C7.

[18] J. Steppan *et al.*, “Arginase modulates myocardial contractility by a nitric oxide synthase 1-dependent mechanism,” *PNAS*, vol. 103, no. 12, pp. 4759–4764, Mar. 2006, doi: 10.1073/pnas.0506589103.

[19] G. Topal, A. Brunet, L. Walch, J.-L. Boucher, and M. David-Dufilho, “Mitochondrial Arginase II Modulates Nitric-Oxide Synthesis through Nonfreely Exchangeable l-Arginine Pools in Human Endothelial Cells,” *J Pharmacol Exp Ther*, vol. 318, no. 3, pp. 1368–1374, Sep. 2006, doi: 10.1124/jpet.106.103747.

[20] T. Schenker, C. Lach, B. Kessler, S. Calderara, and B. Trueb, “A novel GTP-binding protein which is selectively repressed in SV40 transformed fibroblasts.,” *Journal of Biological Chemistry*, vol. 269, no. 41, pp. 25447–25453, Oct. 1994, doi: 10.1016/S0021-9258(18)47271-7.

[21] B. Li and B. Trueb, “DRG represents a family of two closely related GTP-binding proteins,” *Biochimica et Biophysica Acta (BBA) - Gene Structure and Expression*, vol. 1491, no. 1, pp. 196–204, Apr. 2000, doi: 10.1016/S0167-4781(00)00025-7.

[22] K. Ishikawa, S. Azuma, S. Ikawa, K. Semba, and J. Inoue, “Identification of DRG family regulatory proteins (DFRPs): specific regulation of DRG1 and DRG2,” *Genes to cells : devoted to molecular &*

cellular mechanisms, 2005, doi: 10.1111/j.1365-2443.2005.00825.x.

[23] M. S. Ko *et al.*, "Overexpression of DRG2 suppresses the growth of Jurkat T cells but does not induce apoptosis," *Archives of Biochemistry and Biophysics*, vol. 422, no. 2, pp. 137–144, Feb. 2004, doi: 10.1016/j.abb.2003.12.028.

[24] H. Song, "Overexpression of DRG2 Increases G2/M Phase Cells and Decreases Sensitivity to Nocodazole-Induced Apoptosis," *Journal of Biochemistry*, vol. 135, no. 3, pp. 331–335, Mar. 2004, doi: 10.1093/jb/mvh040.

[25] M. S. Ko *et al.*, "Developmentally regulated GTP-binding protein 2 ameliorates EAE by suppressing the development of TH17 cells," *Clinical Immunology*, vol. 150, no. 2, pp. 225–235, Feb. 2014, doi: 10.1016/j.clim.2013.12.004.

[26] M. Mani *et al.*, "Developmentally regulated GTP-binding protein 2 coordinates Rab5 activity and transferrin recycling," *MBoC*, vol. 27, no. 2, pp. 334–348, Jan. 2016, doi: 10.1091/mbc.e15-08-0558.

[27] M. Mani *et al.*, "DRG2 knockdown induces Golgi fragmentation via GSK3β phosphorylation and microtubule stabilization," *Biochimica et Biophysica Acta (BBA) - Molecular Cell Research*, vol. 1866, no. 9, pp. 1463–1474, Sep. 2019, doi: 10.1016/j.bbamcr.2019.06.003.

[28] M.-T. Vo *et al.*, "Developmentally regulated GTP-binding protein 2 depletion leads to mitochondrial dysfunction through downregulation of dynamin-related protein 1," *Biochemical and Biophysical Research Communications*, vol. 486, no. 4, pp. 1014–1020, May 2017, doi: 10.1016/j.bbrc.2017.03.154.

[29] M. Mani *et al.*, "Developmentally regulated GTP-binding protein 2 is required for stabilization of Rac1-positive membrane tubules," *Biochemical and Biophysical Research Communications*, vol. 493, no. 1, pp. 758–764, Nov. 2017, doi: 10.1016/j.bbrc.2017.08.110.

[30] N. A. Yoon *et al.*, "DRG2 supports the growth of primary tumors and metastases of melanoma by enhancing VEGF-A expression," *The FEBS Journal*, vol. 287, no. 10, pp. 2070–2086, 2020, doi: 10.1111/febs.15125.

[31] H. R. Lim *et al.*, "DRG2 Deficient Mice Exhibit Impaired Motor Behaviors with Reduced Striatal Dopamine Release," *International Journal of Molecular Sciences*, vol. 21, no. 1, Art. no. 1, Jan. 2020, doi: 10.3390/ijms21010060.

[32] A. Passaniti, "Extracellular matrix-cell interactions: Matrigel and complex cellular pattern formation," *Lab*

Invest, vol. 67, no. 6, pp. 804; author reply 804-8, Dec. 1992.

[33] L. E. Reynolds *et al.*, "Enhanced pathological angiogenesis in mice lacking β3 integrin or β3 and β5 integrins," *Nat Med*, vol. 8, no. 1, Art. no. 1, Jan. 2002, doi: 10.1038/nm0102-27.

[34] N. Weidner, P. R. Carroll, J. Flax, W. Blumenfeld, and J. Folkman, "Tumor angiogenesis correlates with metastasis in invasive prostate carcinoma.," *Am J Pathol*, vol. 143, no. 2, pp. 401–409, Aug. 1993.

[35] N. A. P. Franken, H. M. Rodermond, J. Stap, J. Haveman, and C. van Bree, "Clonogenic assay of cells in vitro," *Nat Protoc*, vol. 1, no. 5, Art. no. 5, Dec. 2006, doi: 10.1038/nprot.2006.339.

[36] W. C. Aird, "Phenotypic Heterogeneity of the Endothelium," *Circulation Research*, vol. 100, no. 2, pp. 158–173, Feb. 2007, doi: 10.1161/01.RES.0000255691.76142.4a.

[37] Z. Ungvari *et al.*, "Endothelial dysfunction and angiogenesis impairment in the ageing vasculature," *Nat Rev Cardiol*, vol. 15, no. 9, Art. no. 9, Sep. 2018, doi: 10.1038/s41569-018-0030-z.

[38] U. S. Srinivas, B. W. Q. Tan, B. A. Vellayappan, and A. D. Jeyasekharan, "ROS and the DNA damage response in cancer," *Redox Biology*, vol. 25, p. 101084, Jul. 2019, doi: 10.1016/j.redox.2018.101084.

[39] Z. Ungvari, G. Kaley, R. de Cabo, W. E. Sonntag, and A. Csiszar, "Mechanisms of Vascular Aging: New Perspectives," *The Journals of Gerontology: Series A*, vol. 65A, no. 10, pp. 1028–1041, Oct. 2010, doi: 10.1093/gerona/glq113.

[40] Q. Chen, A. Fischer, J. D. Reagan, L. J. Yan, and B. N. Ames, "Oxidative DNA damage and senescence of human diploid fibroblast cells," *PNAS*, vol. 92, no. 10, pp. 4337–4341, May 1995, doi: 10.1073/pnas.92.10.4337.

[41] A. A. Fatokun, T. W. Stone, and R. A. Smith, "Hydrogen peroxide-induced oxidative stress in MC3T3-E1 cells: The effects of glutamate and protection by purines," *Bone*, vol. 39, no. 3, pp. 542–551, Sep. 2006, doi: 10.1016/j.bone.2006.02.062.

[42] Á. Gutiérrez-Uzquiza, M. Arechederra, P. Bragado, J. A. Aguirre-Ghiso, and A. Porras, "p38α Mediates Cell Survival in Response to Oxidative Stress via Induction of Antioxidant Genes: EFFECT ON THE p70S6K PATHWAY*," *Journal of Biological Chemistry*, vol. 287, no. 4, pp. 2632–2642, Jan. 2012, doi: 10.1074/jbc.M111.323709.

[43] Z. Lou and J. Chen, "Cellular senescence and DNA repair," *Experimental Cell Research*, vol. 312, no. 14, pp. 2641–2646, Aug. 2006, doi: 10.1016/j.yexcr.2006.06.009.

[44] J.-P. Coppé *et al.*, “Senescence-Associated Secretory Phenotypes Reveal Cell-Nonautonomous Functions of Oncogenic RAS and the p53 Tumor Suppressor,” *PLOS Biology*, vol. 6, no. 12, p. e301, Dec. 2008, doi: 10.1371/journal.pbio.0060301.

[45] L. He, T. He, S. Farrar, L. Ji, T. Liu, and X. Ma, “Antioxidants Maintain Cellular Redox Homeostasis by Elimination of Reactive Oxygen Species,” *CPB*, vol. 44, no. 2, pp. 532–553, 2017, doi: 10.1159/000485089.

[46] T. Hayashi *et al.*, “Endothelial cellular senescence is inhibited by nitric oxide: Implications in atherosclerosis associated with menopause and diabetes,” *PNAS*, vol. 103, no. 45, pp. 17018–17023, Nov. 2006, doi: 10.1073/pnas.0607873103.

[47] J. H. Kim *et al.*, “Arginase inhibition restores NOS coupling and reverses endothelial dysfunction and vascular stiffness in old rats,” *Journal of Applied Physiology*, vol. 107, no. 4, pp. 1249–1257, Oct. 2009, doi: 10.1152/japplphysiol.91393.2008.

[48] W. Shin, D. E. Berkowitz, and S. Ryoo, “Increased arginase II activity contributes to endothelial dysfunction through endothelial nitric oxide synthase uncoupling in aged mice,” *Exp Mol Med*, vol. 44, no. 10, Art. no. 10, Oct. 2012, doi: 10.3858/emm.2012.44.10.068.

[49] J. W. Ashby and J. J. Mack, “Endothelial Control of Cerebral Blood Flow,” *The American Journal of Pathology*, vol. 191, no. 11, pp. 1906–1916, Nov. 2021, doi: 10.1016/j.ajpath.2021.02.023.

[50] A. J. Donato, R. G. Morgan, A. E. Walker, and L. A. Lesniewski, “Cellular and molecular biology of aging endothelial cells,” *Journal of Molecular and Cellular Cardiology*, vol. 89, pp. 122–135, Dec. 2015, doi: 10.1016/j.yjmcc.2015.01.021.

[51] G. P. Dimri *et al.*, “A biomarker that identifies senescent human cells in culture and in aging skin in vivo,” *PNAS*, vol. 92, no. 20, pp. 9363–9367, Sep. 1995, doi: 10.1073/pnas.92.20.9363.

[52] J.-P. Coppé, P.-Y. Desprez, A. Krtolica, and J. Campisi, “The senescence-associated secretory phenotype: the dark side of tumor suppression,” *Annu Rev Pathol*, vol. 5, pp. 99–118, 2010, doi: 10.1146/annurev-pathol-121808-102144.

[53] T. Lu and T. Finkel, “Free radicals and senescence,” *Experimental Cell Research*, vol. 314, no. 9, pp. 1918–1922, May 2008, doi: 10.1016/j.yexcr.2008.01.011.

[54] P. Rai *et al.*, “Continuous elimination of oxidized nucleotides is necessary to prevent rapid onset of cellular senescence,” *PNAS*, vol. 106, no. 1, pp. 169–174, Jan. 2009, doi: 10.1073/pnas.0809834106.

[55] F. Bringold and M. Serrano, “Tumor suppressors and oncogenes in cellular senescence☆,” *Experimental Gerontology*, vol. 35, no. 3, pp. 317–329, May 2000, doi: 10.1016/S0531-5565(00)00083-8.

[56] B. Liu, Y. Chen, and D. K. St. Clair, “ROS and p53: A versatile partnership,” *Free Radical Biology and Medicine*, vol. 44, no. 8, pp. 1529–1535, Apr. 2008, doi: 10.1016/j.freeradbiomed.2008.01.011.

[57] C. J. Sherr and J. M. Roberts, “CDK inhibitors: positive and negative regulators of G1-phase progression,” *Genes Dev.*, vol. 13, no. 12, pp. 1501–1512, Jun. 1999.

[58] H. Cai and D. G. Harrison, “Endothelial Dysfunction in Cardiovascular Diseases: The Role of Oxidant Stress,” *Circulation Research*, vol. 87, no. 10, pp. 840–844, Nov. 2000, doi: 10.1161/01.RES.87.10.840.

[59] U. Förstermann *et al.*, “Nitric oxide synthase isozymes. Characterization, purification, molecular cloning, and functions.,” *Hypertension*, vol. 23, no. 6_pt_2, pp. 1121–1131, Jun. 1994, doi: 10.1161/01.HYP.23.6.1121.

[60] D. Stuehr, S. Pou, and G. M. Rosen, “Oxygen Reduction by Nitric-oxide Synthases*,” *Journal of Biological Chemistry*, vol. 276, no. 18, pp. 14533–14536, Jan. 2001, doi: 10.1074/jbc.R100011200.

[61] U. Landmesser *et al.*, “Oxidation of tetrahydrobiopterin leads to uncoupling of endothelial cell nitric oxide synthase in hypertension,” *J Clin Invest*, vol. 111, no. 8, pp. 1201–1209, Apr. 2003, doi: 10.1172/JCI14172.

[62] T. Bachetti *et al.*, “Arginase pathway in human endothelial cells in pathophysiological conditions,” *Journal of Molecular and Cellular Cardiology*, vol. 37, no. 2, pp. 515–523, Aug. 2004, doi: 10.1016/j.yjmcc.2004.05.004.

APPENDIX

Le, Anh-Nhung, Seong-Soon Park, Minh-Xuan Le, Unn Hwa Lee, Byung Kyun Ko, Hye Ryeong Lim, Ri Yu, Seong Hee Choi, Byung Ju Lee, Soo-Youn Ham, Chang Man Ha, and Jeong Woo Park. 2022. "**DRG2 Depletion Promotes Endothelial Cell Senescence and Vascular Endothelial Dysfunction**." International Journal of Molecular Sciences 23(5):2877. doi: 10.3390/ijms23052877.